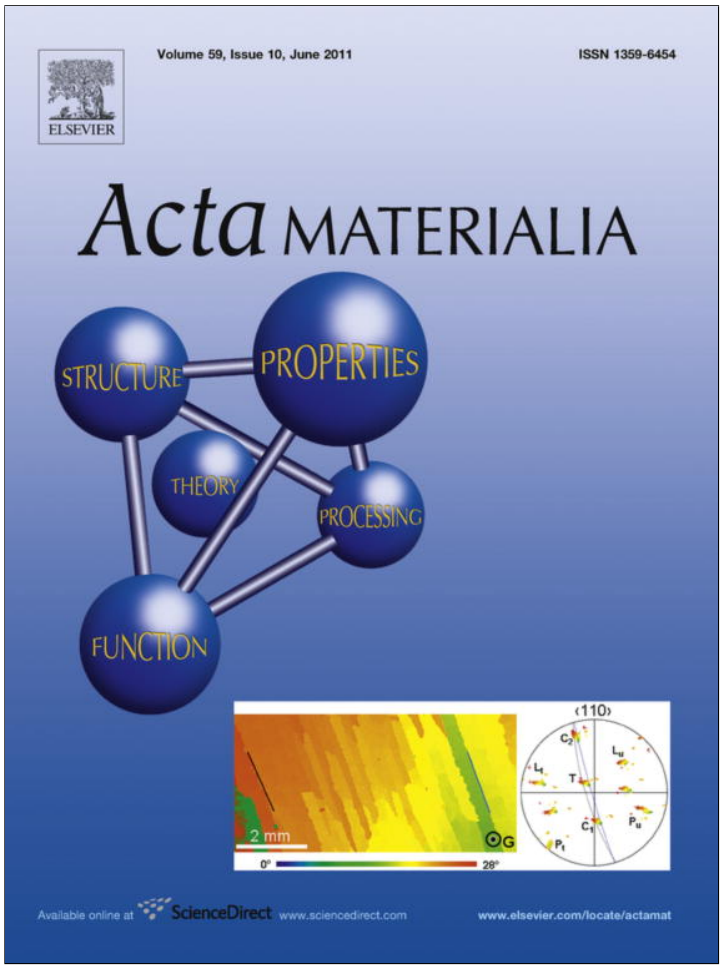

Available online at www.sciencedirect.com
ScienceDirect
Acta Materialia 59 (2011) 3883–3894
Acta MATERIALIA
www.elsevier.com/locate/actamat

Atomistic study of the buckling of gold nanowires

Pär A.T. Olsson [a,*], Harold S. Park [b]

[a] Division of Mechanics, Lund University, PO Box 118, SE-221 00 Lund, Sweden
[b] Department of Mechanical Engineering, Boston University, Boston, MA 02215, USA

Received 25 November 2010; received in revised form 25 January 2011; accepted 6 March 2011
Available online 12 April 2011

Abstract

In this work, we present results from atomistic simulations of gold nanowires under axial compression, with a focus on examining the effects of both axial and surface orientation effects on the buckling behavior. This was accomplished by using molecular statics simulations while considering three different crystallographic systems: ⟨100⟩/{100}, ⟨100⟩/{110} and ⟨110⟩/{110}{100}, with aspect ratios spanning from 20 to 50 and cross-sectional dimensions ranging from 2.45 to 5.91 nm. The simulations indicate that there is a deviation from the inverse square length dependence of critical forces predicted from traditional linear elastic Bernoulli–Euler and Timoshenko beam theories, where the nature of the deviation from the perfect inverse square length behavior differs for different crystallographic systems. This variation is found to be strongly correlated to either stiffening or increased compliance of the tangential stiffness due to the influence of nonlinear elasticity, which leads to normalized critical forces that decrease with decreasing aspect ratio for the ⟨100⟩/{100} and ⟨100⟩/{110} systems, but increase with decreasing aspect ratio for the ⟨110⟩/{110}{100} system. In contrast, it was found that the critical strains are all lower than their bulk counterparts, and that the critical strains decrease with decreasing cross-sectional dimensions; the lower strains may be an effect emanating from the presence of the surfaces, which are all more elastically compliant than the bulk and thus give rise to a more compliant flexural rigidity.

Keywords: Buckling; Nanowire; Molecular statics

1. Introduction

In recent years, extensive research efforts have been devoted to increasing the understanding of the mechanical properties of nanowires. The underlying reason for this is because nanowires are potential candidates as components in future nanoelectromechanical systems (NEMS) [1–3]. Furthermore, due to their nanometer dimensions, nanostructures tend to display physical properties that often differ markedly from that of macroscopic structures. The basic reason for this is because surface atoms have a different bonding environment due to their reduced coordination as compared to bulk atoms, which results in the enhancement of non-bulk physical properties with decreasing nanostructure size, or increasing surface area to volume ratio [2,3].

Experimentally, the elastic properties of nanowires are usually determined either through bending [4–10], tensile [11,12] or dynamic resonant experiments [3,13–25], where the elastic properties are extracted from the continuum mechanical relations connecting the deflection, strain, force or resonant properties with the Young's modulus. Recently, another mechanical testing technique, that of buckling, has been utilized, where the elastic properties are obtained by determining the critical force needed to cause buckling instability of the nanowires in compression, and subsequently relating the critical force to existing continuum relations from which the elastic properties are extracted [26–29].

The elastic stability and behavior of nanowires under compression have also become critical for other applications. For example, recent experiments on gold nanowires with cross-sectional dimensions as small as 3 nm have

* Corresponding author. Tel.: +46 46 2223865; fax: +46 46 2224620.
E-mail addresses: par.olsson@mek.lth.se (P.A.T. Olsson), parkhs@bu.edu (H.S. Park).

1359-6454/$36.00 © 2011 Acta Materialia Inc. Published by Elsevier Ltd. All rights reserved.
doi:10.1016/j.actamat.2011.03.012

shown that nanowires can be joined together through cold welding. This occurs through the pressing together of two nanowires, resulting in welding through atomic diffusion at the interface of the nanowires [30]. For this application, it is essential that the nanowires are not exposed to overly large compressive forces, as the stability, and thus the ability to cold weld the nanowires may be degraded. Nanowires under the influence of axial strain have also attracted increasing interest lately as one may mechanically tune the resonant frequencies using tensile or compressive strains. This is important as it opens up the possibility of creating high-quality-factor micro- and nanoresonators with variable eigenfrequency spectra suitable for a number of applications [23–25,31,32]. However, if the compressive force or strain exceeds the critical force or strain, then the nanowire may not vibrate controllably due to the onset of buckling instability. Finally, recent developments have paved the way for employment of highly flexible and stretchable electronics [33,34], which are now beginning to utilize wavy, buckled nanowires that can undergo significant amounts of stretching before plastic deformation occurs. In this type of application, surface effects on the nanowires and their buckling behavior and properties may play a central role in the performance of the devices.

These applications all demonstrate that it is critical to investigate and understand not only how nanowires behave under the influence of compressive loads, but also to study how well critical loads and strains predicted from traditional continuum mechanics agree with those obtained from direct atomistic modeling of the surface-dominated nanowires.

Molecular dynamics and molecular statics (MS) have been popular numerical tools for simulating mechanical properties of nanowires and have revealed many interesting features such as elastic size and crystallographic dependence, asymmetric yielding properties, nonlinear elastic properties, shape memory, spontaneous phase transformations due to surface stress, pseudoelastic behavior, etc. [31,32,35–54]. When considering buckling properties, most atomistic simulations have shown that the critical strains and forces are found to be significantly larger than what can be predicted from fundamental Bernoulli–Euler buckling predictions [49–52]. Moreover, there have been reports of the critical strain being dependent on the applied strain increment size and it has been found that the stress–strain and energy–strain curves may become discontinuous when buckling occurs [47–54]. Strain increment size dependencies and discontinuous energy–strain curves imply that the transition between the straight beam to the buckled beam does not necessarily follow the lowest energy path, which complicates the extraction of the critical buckling force and strain at which the straight-beam configuration becomes unstable. We also note that the literature on the buckling of nanowires is considerably less well-developed than the extensive literature on the buckling of carbon nanotubes.

The purpose of this paper is to study, using MS simulations, the effects of nanowire size, axial orientation and surface orientation on the buckling properties of gold nanowires, and to evaluate how well the critical loads and strains predicted from traditional continuum mechanics as well as recently developed surface elasticity theories [55] agree with our simulation results. In addition to the buckling studies, we detail a simple procedure that we have utilized to address the issues regarding strain increment dependencies and discontinuous energy–strain and stress–strain curves that have been observed from previous atomistic studies of nanostructure buckling [47,51–54].

2. Preliminaries

For slender beams loaded in compression, the load-carrying ability and the geometry of the beam are highly dependent on the magnitude of the compressive force. For small loads, the geometry and the load-carrying ability are not prone to undergo any noticeable changes and the state is considered to be stable. However, increasing the compressive force will eventually lead to a threshold value at which the straight-beam equilibrium configuration becomes unstable. This means that a small lateral force or asymmetry will induce bowing deformations which will not disappear despite removal of the lateral force, which may result in loss of load-carrying ability for the beam. In classical elasticity theory, the critical load for an ideal doubly clamped Bernoulli–Euler beam is written as:

$$F_{cr} = -\frac{4\pi^2 (EI)^*}{L^2}, \tag{1}$$

where L denotes the length of the beam and $(EI)^*$ is the flexural rigidity, which is given by:

$$(EI)^* = \int_A Ez^2 dA, \tag{2}$$

where E denotes Young's modulus and z is the coordinate normal to the plane spanned by the wire axis and the cross-sectional rotation axis, measured from the neutral axis. For a homogeneous cross-section, the critical strain can be written as:

$$\epsilon_{cr} = -\frac{4\pi^2 I}{AL^2}, \tag{3}$$

where we have used the linear elastic relation between stress and strain, which is valid for strains in the linear elastic regime, and A and I are the cross-sectional area and moment of inertia, respectively [56]. The minus signs in Eqs. (1) and (3) indicate that the critical forces and strains are compressive. We note that Eq. (3) demonstrates that, in the macroscopic continuum beam theory where the cross-sections are assumed to be homogeneous, the critical strain is only a function of the beam geometry, and not of the elastic properties.

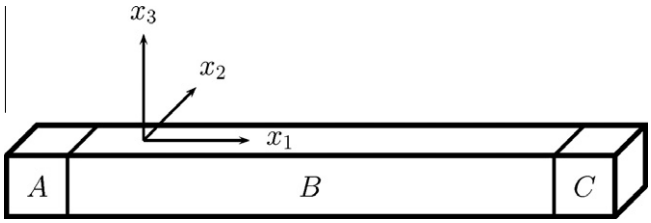

Fig. 1. Schematic view of the nanowire in the simulations.

Table 1
Cross-sectional sizes in the format $h \times w$ in nm^2 for the simulated nanowires.

⟨100⟩/{100}	⟨100⟩/{110}	⟨110⟩/{110}{100}
2.45 × 2.45	2.45 × 2.45	3.32 × 3.47
3.26 × 3.26	3.32 × 3.32	4.18 × 4.28
4.08 × 4.08	4.18 × 4.18	5.91 × 5.92
5.71 × 5.71	5.91 × 5.91	

3. Numerical details

3.1. Geometries

The considered nanowires are defect-free gold single crystals with cross-sections as close to perfect squares as possible. Three types of systems are considered, where the orthogonal directions (x_1,x_2, x_3) in Fig. 1 correspond to the ([100], [010], [001]), ([100], [011], [0$\bar{1}$1]) and ([110], [001], [1$\bar{1}$0]) directions so that two different types of free surfaces are considered, i.e. {100} and {110} surfaces, and two different types of axial directions are investigated, i.e. ⟨100⟩ and ⟨110⟩. These systems will subsequently be referred to as ⟨100⟩/{100},⟨100⟩/{110} and ⟨110⟩/{110}{100} systems, respectively. The considered cross-sectional sizes can be seen in Table 1 for the different systems and we have considered aspect ratios ranging from 20 to 50.

The atomistic systems are divided into three different regions, A, B and C, as illustrated in Fig. 1. Regions A and C are boundary regions whose main purpose are to mimic doubly clamped boundary conditions. Region B consists of free atoms which constitute the actual nanowire, hence the length of nanowire is the same as the measured length of region B. The lengths of regions A and C differ for different simulations but they were chosen to be no less than four lattice constants long each, which is sufficiently long so that region B is not influenced by the free end surfaces.

3.2. MS simulations

MS simulations are performed for the numerical part of this work and the simulations are conducted as follows. First we let the nanowire relax to a potential energy minimum using the FIRE algorithm [57], where throughout this initial minimization all the atoms are allowed to move freely without any constraints, except for the atoms in region A in Fig. 1 which are fixed throughout the entire simulation. This relaxation step was performed such that the atoms could find new equilibrium positions in response to the surface stress that acts on the nanowire; the new equilibrium configuration corresponds to a reduction in the nanowire length of the order of 1–3% depending on the cross-sectional size, surrounding surfaces and axial orientation.

Once this initially relaxed stress-free state of equilibrium was found, the atoms in region C were translated in the negative x_1 direction and held fixed, while the free atoms in B were allowed to move to the potential-energy-minimizing positions using the FIRE algorithm. This displacement-controlled compressive straining procedure was repeated several times so that the stress measured in region B and the reaction force acting on region C could be measured as a function of the strain. In all the simulations we consistently measure the strains from the initially relaxed state where the nanowire length has been reduced due to the surface stresses, so that the zero strain state corresponds to that where the axial stress has been balanced. This means that the ideal interplanar distance along the wire axis, in general, does not correspond to the zero strain state. The convergence criterion was chosen so that convergence was assumed to be met when the root-mean-square force of the system was less than 10^{-11} eV/Å. The interatomic interaction is modeled through an embedded atom method (EAM) potential, fitted to gold properties [58]. This potential describes the elastic properties of gold very well, which is of great importance in this study.

Importantly, the above numerical scheme alone is not sufficient for calculating the critical force and strain as the amount of force and strain at which the nanowires buckle depends on the displacement increment size. Moreover, there is no guarantee that the nanowire will buckle as opposed to deform plastically if the simulation is performed this way, even when the critical buckling strain is less than the yield strain. This type of arbitrary behavior can also be observed in previous atomistic studies of nanostructure buckling [47–54], but no explanation of, or remedy to, the problem has previously been given.

The reason behind this increment dependence is the high symmetries of the systems which lead to unstable states of equilibria and small potential energy gradients. Due to the small potential energy gradients, the minimization algorithm may not be able to leave the unstable straight-beam equilibrium configuration in favor of the more stable minimum energy state with bowing deformations. Hence the obtained transition does not necessarily follow the minimum potential energy path but is rather governed by chance. To overcome this complication, a perturbation was employed to break the symmetry, and this was done by perturbing the potential energy gradient by adding small additional external forces acting on the free atoms in region B so that the resulting force on the free atoms is written as:

$$\mathbf{F}_i = -\frac{\partial \Phi}{\partial \mathbf{r}_i} + \delta \mathbf{F}, \tag{4}$$

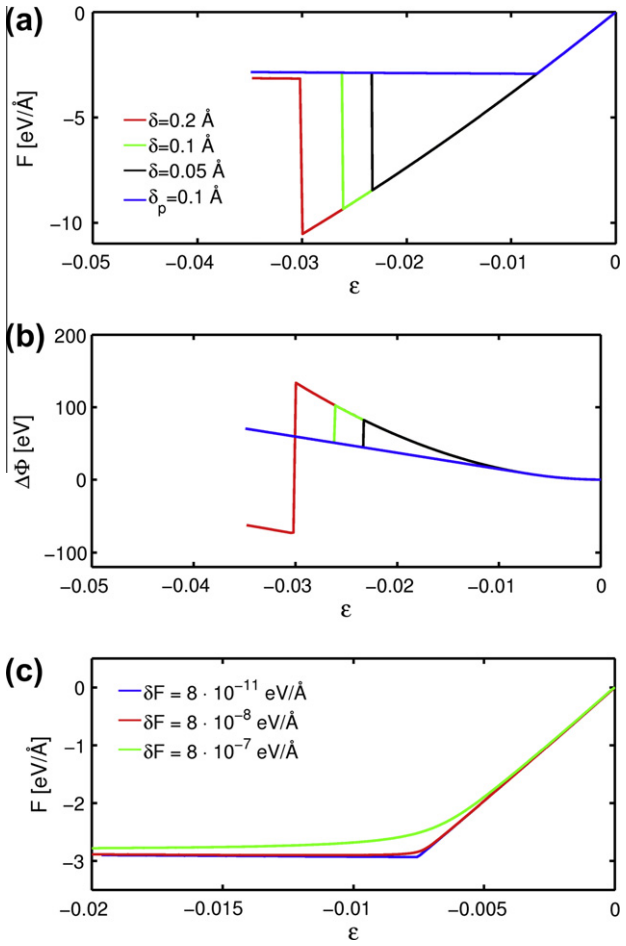

Fig. 2. Illustration of increment dependence of (a) the critical force and (b) potential energy for perturbed and unperturbed systems as function of strain. The perturbed system is denoted δ_p and the unperturbed systems are denoted δ. (c) Perturbation magnitude convergence study. (For interpretation to colours in this figure, the reader is referred to the web version of this paper.)

where Φ denotes the total potential energy and the vector $\delta\mathbf{F} = (0, \delta F, \delta F)$ is the perturbation which is employed to disturb the symmetry of the system. This means that the minimization algorithm will find a slightly different state of equilibrium than what would be found if we minimize the potential energy. However, if we choose δF small enough, as we will discuss further in Section 3.3, this difference is negligible.

3.3. Numerical evaluation

In Fig. 2 we have illustrated the resulting differences between simulations with and without employment of perturbations and also the influence of the perturbation size on the force–strain behavior. In Fig. 2a we have compared the force–strain curves for perturbed and unperturbed systems, and, as previously mentioned, for the unperturbed systems we found that the type of instability which occurs and the critical point at which instability occurs are highly dependent on the strain increment size. In fact, the unperturbed systems buckled when the increment sizes were $\delta = 0.05$ Å and $\delta = 0.1$ Å; however, when $\delta = 0.2$ Å, the nanowire deformed plastically (cf. Fig. 3). When we did perturb the system ($\delta_p = 0.1$ Å) the instability occurred at a lower strain and, unlike for the unperturbed simulations, the obtained force–strain curve is not discontinuous. Even though we have only reported results from one simulation where a perturbation has been employed in this evaluation, several simulations were performed with different strain increment sizes and the resulting buckling properties from those simulations did not show any strain increment size dependence.

We have also compared the energy–strain curves for perturbed and unperturbed systems (cf. Fig. 2b). As can be seen, the energy–strain curves for the unperturbed systems are discontinuous in the same manner as for the force–strain curves, whereas the curve of the perturbed system is continuous. In fact, it is seen that the energy curve which corresponds to the lowest-energy transition path is the curve of the perturbed system. Hence, that path is the most likely transition path to occur, supporting the conjecture that the symmetry needs to be broken in order for the lowest-energy transition to occur. From Fig. 2a it can be seen that the force curve becomes almost perfectly horizontal at the critical point. The axial stress is related to the potential energy curve through:

$$\sigma = \frac{F}{A} = \frac{1}{V}\frac{d\Phi}{d\epsilon}, \tag{5}$$

which means that when the force curve becomes horizontal, the potential energy curve becomes a linear function of the strain. Thus, the energy curve transitions from a parabolic function to a linear function at the critical point, which can be confirmed by inspection of Fig. 2b.

Moreover, in Fig. 2c we have performed a perturbation convergence study to monitor the influence of the perturbation magnitude on the buckling properties. In the production simulations the perturbations were chosen to be of the order $10^{-11} < \delta F < 10^{-9}$ eV/Å, which were found to be sufficiently large to get the nanowires to buckle and small enough not to influence the response notably. The sizes of these perturbations are very small even in the context of atomistic simulations, up to roughly 100 times the convergence criterion we utilized, where the root-mean-square convergence tolerance for the system force was set to be less than 10^{-11} eV/Å. We monitored the total potential energy of the nanowire and the potential energy of the individual atoms both for perturbed and unperturbed systems up to the critical point, and the differences were found to be of the order of 0.1–1 ppm. This shows that the influence of the perturbation on the mechanical properties of the surfaces and the bulk is negligible. Nevertheless, they are essential in order to get the nanowires to buckle at the critical point.

Even though some of the considered perturbations in Fig. 2c are much exaggerated, larger than roughly 100 times the perturbations that were used in the production runs, they illustrate how the transition character changes

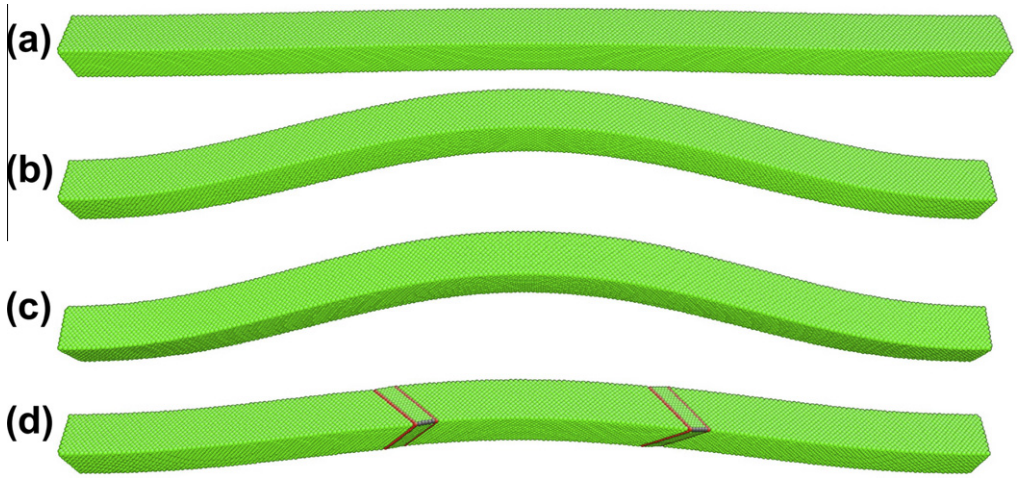

Fig. 3. Nanowires subjected to different strain increments after instability has occurred for (a) $\delta_p = 0.1$ Å, (b) $\delta = 0.05$ Å, (c) $\delta = 0.1$ Å and (d) $\delta = 0.2$ Å. The atoms are characterized using the method proposed by Ackland and Jones [59] (green = fcc, red = hcp, gray = unknown). The figures are generated using AtomEye software [60]. (For interpretation of the references to colour in this figure legend, the reader is referred to the web version of this article.)

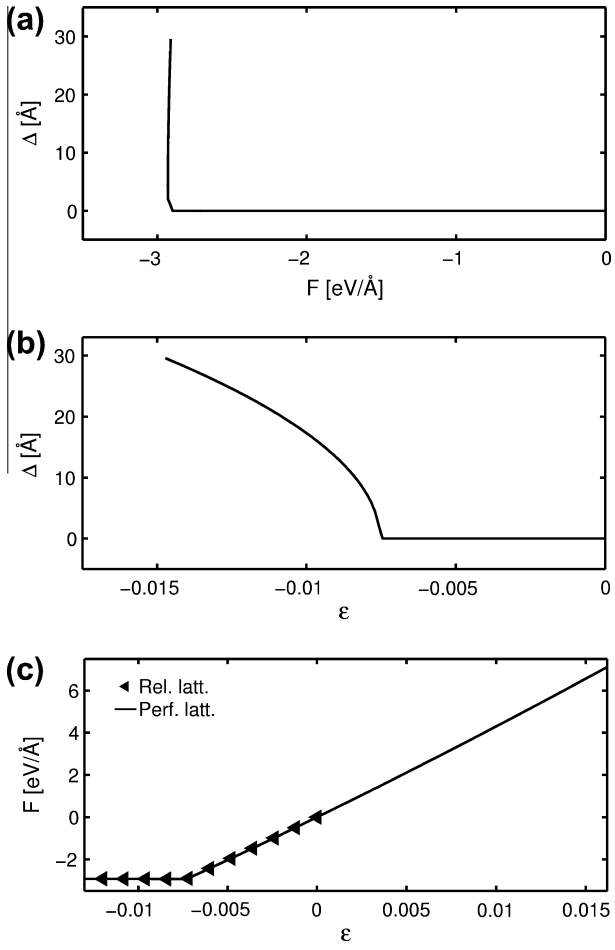

Fig. 4. (a) The deflection of the midpoint of the nanowire cross-section as a function of the compressive axial force and (b) the deflection of the midpoint as a function of the applied axial strain. (c) Comparison of straining from two different initial conditions, the solid line corresponds to straining from perfect lattice distance and the markers correspond to straining from the relaxed state.

when the nanowire is subjected to a perturbation that is too large; even though the critical force remains essentially unchanged it becomes harder to distinguish any distinct point of instability. Thus, it becomes more difficult to extract the critical strain with high accuracy when the perturbation is too large.

In Figs. 4a and b, we have compared the deflection of the midpoint of a nanowire as functions of the axial force and axial strain, respectively. From Fig. 4b it can be seen that increasing the compressive axial strain does not result in any buckling-type deflections until a critical strain is reached. Once the critical strain is reached, the deflections increase significantly. Furthermore, from Fig. 4a it is observed that the axial force reaches a threshold value after which the axial force does not increase even if the axial strain is increased. However, if the axial strain is increased, the deflection is also increased. These observations are confirmations that it is indeed buckling that occurs and that the numerical scheme presented is appropriate for finding the critical strains and loads.

Finally, in Fig. 4c we have investigated if the buckling properties depend on which state we start to compress the nanowire from. We did compress nanowires from the relaxed state, where the nanowires have been allowed to contract to balance the surface stresses, and from the ideal state where the initial interplanar distance along the wire axis corresponds to the ideal; note that Fig. 4c shows that the compressive relaxation strain due to surface stress effects (i.e. in the absence of any external loading) for the particular nanowire considered in Fig. 4 is about 1.62%. From Fig. 4c it can be seen that these two curves coincide and thus the buckling properties do not depend on which of the two initial configurations the nanowires are loaded from. Consistently throughout this paper, we consider the relaxed state to be the initial configuration.

4. Results and discussion

4.1. Critical buckling forces

We have adopted two different approaches when evaluating the critical forces. First, we have compared critical forces of different cross-sectional dimensions with the inverse square aspect ratio. The reason for this can be deduced from Eq. (1), where it is seen that the critical buckling force is proportional to the inverse square length of the nanowire. Thus, in Fig. 5 we have plotted the critical load for different cross-sections against the inverse square aspect ratio to study how well this behavior is satisfied. Second, we have also studied the normalized critical buckling forces (cf. Fig. 6). Here we have made the critical force dimensionless, by instead considering the quantity $|F_{cr}|L^2/(4\pi^2 E_b I)$, where E_b is the Young's modulus of the bulk, which has values of 46.1 and 87.9 GPa for the ⟨100⟩ and ⟨110⟩ directions, respectively, I is the moment of inertia, and $|F_{cr}|$ is the magnitude of the critical force measured from the MS simulations. This dimensionless quantity is the same as the ratio between the obtained critical force and that of the bulk, and sheds light on other important issues such as elastic cross-sectional size and aspect ratio dependencies.

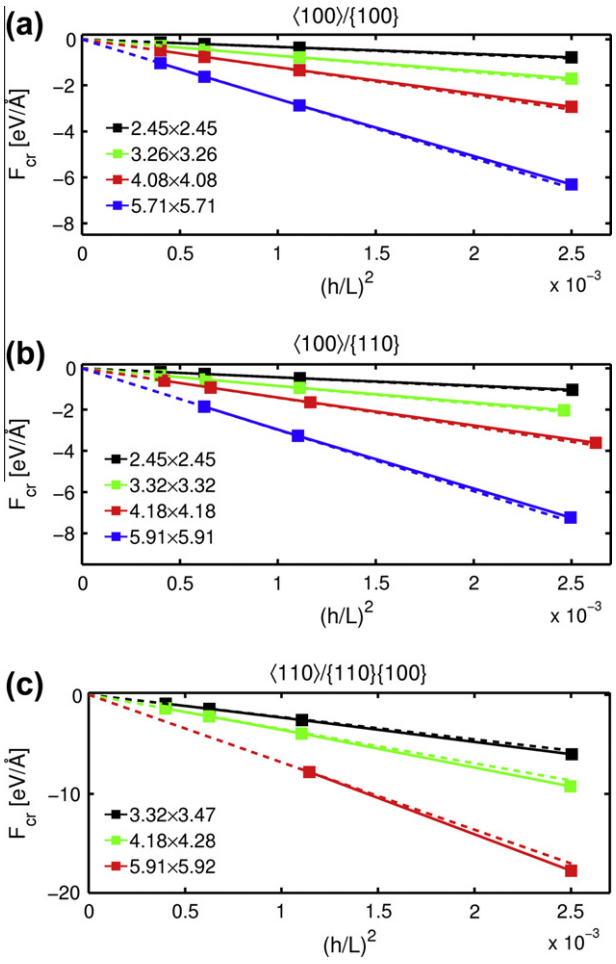

Fig. 5. The critical buckling force vs. the inverse square aspect ratio for (a) ⟨100⟩/{100}, (b) ⟨100⟩/{110} and (c) ⟨110⟩/{110}{100} systems. The dashed lines are perfectly linear curves through the origin and the point with the lowest value of $(h/L)^2$ for the corresponding cross-section to distinguish any deviations from the ideal inverse square length dependence. (For interpretation to colours in this figure, the reader is referred to the web version of this paper.)

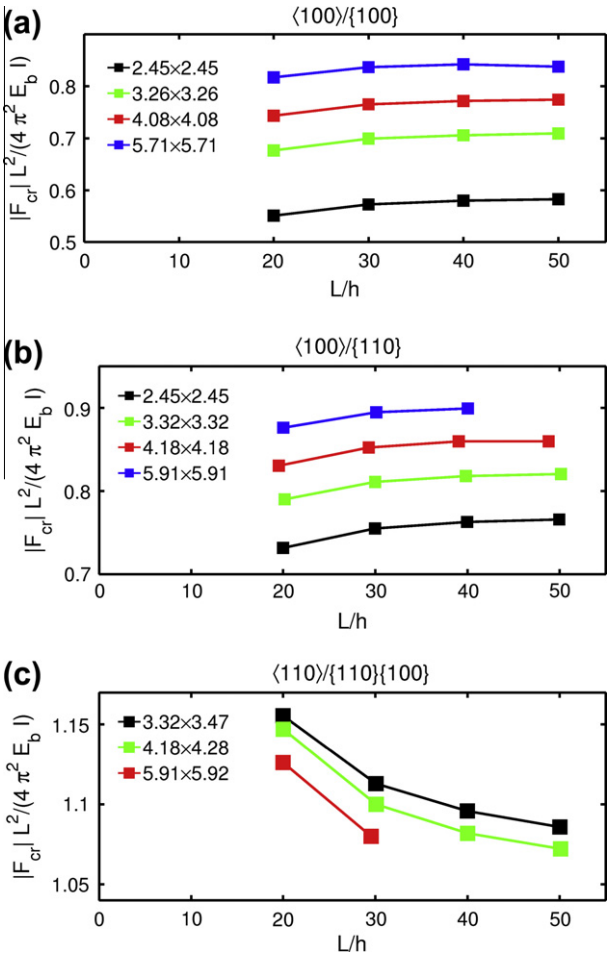

Fig. 6. Normalized critical buckling force as functions of the aspect ratio for (a) ⟨100⟩/{100}, (b) ⟨100⟩/{110} and (c) ⟨110⟩/{110}{100} systems. (For interpretation to colours in this figure, the reader is referred to the web version of this paper.)

From Fig. 5 it can be seen that the curves are quite close to linear going through the origin. This is of course what is expected from Eq. (1). Although it is hard to distinguish any deviations of the curves in Fig. 5 from linearity going through the origin, it appears that for nanowires with small aspect ratios, i.e. when $(h/L)^2$ is large, the deviations from perfectly linear curves through the origin increase. This observation can be confirmed from Fig. 6, where it is seen that the curves are not perfectly horizontal which reveals an unexpected aspect ratio dependence. It is shown that the critical buckling force decreases for ⟨100⟩/{100} and ⟨100⟩/{110} nanowires, while it increases with decreasing aspect ratio for the ⟨110⟩/{110}{100} nanowires. Moreover, it can be seen that the curves in Fig. 6 are not overlapping and this is an indication that there is a cross-sectional size dependence in the flexural rigidity. We will address these two issues separately.

4.1.1. Cross-sectional size dependence

It is well known that the introduction of surfaces and axial relaxations leads to elastic properties that deviate from those of the bulk [45,61,62]. In particular, it has been found that the Young's modulus decreases with decreasing cross-sectional size for nanowires when the axial direction corresponds to a ⟨100⟩ direction, whereas for ⟨110⟩ directions it has been found that the Young's modulus increases with decreasing cross-sectional size [45,61,62]. Because of the close relation between flexural rigidity and Young's modulus through Eq. (2), if the Young's modulus varies with the cross-sectional size, this will also influence the critical buckling force. In Fig. 6 it is seen that the curves are not overlapping but rather differ in terms of magnitude. For ⟨100⟩/{100} and ⟨100⟩/{110} nanowires the normalized critical forces are less than 1 for all the considered nanowires and decrease with decreasing cross-sectional size, whereas for ⟨110⟩/{110}{100} nanowires we find that the normalized critical forces are larger than what is predicted by the bulk and are increasing with decreasing cross-sectional size. Hence, the overall trends of the cross-sectional size dependence observed for Young's modulus by previous researchers are in accordance with the observed cross-sectional size dependence of the normalized critical forces in this work.

When comparing the curves in Figs. 6a and b it should be noted that both of the considered systems have the same ⟨100⟩ axial orientation but different types of bounding surfaces, i.e. {100} and {110} surfaces, respectively, which makes it possible to study if and how the surfaces influence the critical buckling forces. Comparing the systems with the cross-section size $2.45 \times 2.45\ \text{nm}^2$ it can be seen that the critical forces for the ⟨100⟩/{100} system are between 50% and 60% of the corresponding bulk value, while for the ⟨100⟩/{110} system the critical forces fall between 70% and 80% of the corresponding bulk value. Hence, the critical forces for the ⟨100⟩/{110} system are clearly higher than for the ⟨100⟩/{100} system, which is a general observation for all the considered cross-sections in Figs. 6a and b.

We did extract the Young's modulus for both the ⟨100⟩/{100} and ⟨100⟩/{110} systems for the nanowires with the cross-section size $2.45 \times 2.45\ \text{nm}^2$ from the linear elastic regime of the stress–strain curves and they were found to be 31.5 and 42.1 GPa, respectively. Since the bulk value is 46.1 GPa, this means that the presence of {100} surfaces leads to a more compliant structure than the {110} surfaces, which can also be observed by comparison of Figs. 6a and b. The ratios between these finite-sized values of the Young's modulus and the bulk value are 68% and 91% for the ⟨100⟩/{100} and ⟨100⟩/{110} systems, respectively. However, these ratios are higher than the normalized critical forces which were in the range 50–60% and 70–80%, respectively, which means that the cross-sectional size dependencies of the normalized critical forces can only partly be attributed to the cross-sectional size dependencies of the Young's modulus for the ⟨100⟩/{100} and ⟨100⟩/{110} systems. This observation was found to be true for all the cross-sectional sizes.

For the ⟨110⟩/{110}{100} system, extracting the Young's modulus from the linear elastic regime yielded a value of 100.1 GPa for nanowires with a $3.32 \times 3.47\ \text{nm}^2$ cross-section. The ratio between this value and the corresponding bulk value, 87.9 GPa, is 1.14, which is in quite good agreement with the normalized critical forces of 1.16 and 1.11 for nanowires with aspect ratios 20 and 30, respectively. However, there are increasing discrepancies when comparing with nanowires with greater aspect ratios as it can be seen that the normalized critical forces are less than 1.1 in the limit of large aspect ratios. It can thus be concluded that in the limit of large aspect ratios, the normalized critical forces are smaller than the ratio between the cross-sectional size-dependent Young's modulus and the Young's modulus of the bulk for all crystallographic orientations. We will address this further in Section 4.3. Comparing the different systems, it is found that the deviations are smaller than for the ⟨100⟩/{100} and ⟨100⟩/{110} systems, which implies that a large part of the cross-sectional size dependencies of the normalized critical forces for the ⟨110⟩/{110}{100} systems can be attributed to the cross-sectional size dependence of Young's modulus, which is in contrast to what was observed for the ⟨100⟩/{100} and ⟨100⟩/{110} systems.

4.1.2. Aspect ratio dependence

Given the aforementioned cross-sectional size dependence of the Young's modulus, theoretically all the curves in Fig. 6 should be perfectly horizontal. The reason behind this is that the ratio $|F_{cr}|L^2/(4\pi^2 E_b I)$ is merely the ratio between the flexural rigidity of the nanowire and that of the ideal bulk. The flexural rigidity is a cross-sectional property and depends on the cross-sectional geometry and the Young's modulus, and we do not expect the Young's modulus to vary with the nanowire length. Thus it is expected that the flexural rigidity will be constant for a specific cross-sectional size with the aspect ratios that we have considered in this paper, and that the curves in Fig. 6 should be perfectly horizontal. As can be seen, there are some deviations in the normalized critical force from being perfectly horizontal. This implies that there is a slight aspect ratio dependence which is not accounted for by Eq. (1). It is also observed that the normalized critical forces for the specific cross-sections do appear to approach an asymptotic limit value as the aspect ratio increases. Nevertheless, on most accounts these deviations are quite small and it appears as if the curves in Fig. 6 do not deviate significantly from horizontal curves and the variations between aspect ratios 20 and 50 are less than 7%. Thus, for the studied nanowires in this work, this deviation is not as important as the cross-sectional size dependence of the Young's modulus in causing deviations of the critical buckling force from the expected bulk value.

Although it is unlikely that shearing will have any significant influence on the buckling properties of nanowires

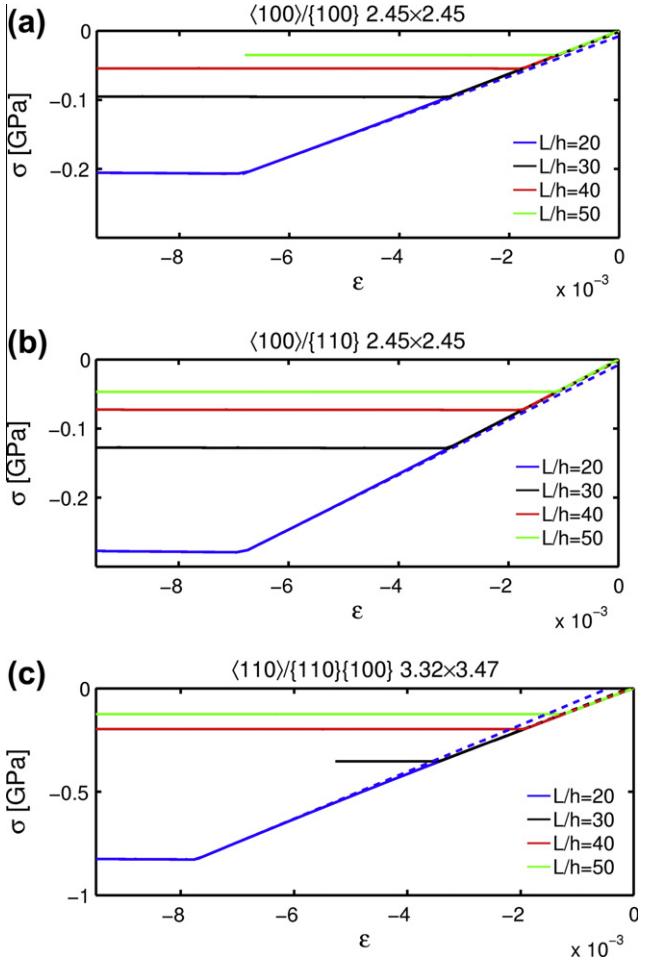

Fig. 7. The solid lines are stress–strain curves for (a) ⟨100⟩/{100}, (b) ⟨100⟩/{110}, and (c) ⟨110⟩/{110}{100} systems. The dashed curves corresponds to the tangential stiffness of the stress–strain curves just before buckling occurs. (For interpretation to colours in this figure, the reader is referred to the web version of this paper.)

with aspect ratios greater or equal to 20, we have employed Timoshenko beam theory [63] to see whether this is an effect due to shearing. It turned out that the influence was minimal and certainly much smaller than the deviations from perfectly horizontal curves that can be seen in Fig. 6, and so does not explain why the curves are not horizontal.

If we study the separate figures, i.e. Figs. 6a–c, it can be seen that the curves in each part seem to follow the same trends and appear to look very similar except for the fact that they are translated along the y-axis. What is also interesting is that the greatest deviation seems to be attained for nanowires with the smallest aspect ratios. Taking Eq. (3) as the starting point, it can be deduced that the critical strain for systems with square cross-sections is given by $(-\pi^2/3)(h/L)^2$. Therefore, ideally, the critical strains will be −0.82%, −0.36%, −0.21% and −0.13% for nanowires with aspect ratios 20, 30, 40 and 50, respectively. It is therefore clear that larger compressive strains are needed for smaller aspect ratio nanowires in order to reach the point of buckling, which implies that nonlinear elastic contributions appear to become increasingly important for nanowires with small aspect ratios.

To investigate this in more detail, we studied stress–strain curves to see whether there are any variations from perfectly linear elastic behavior. In addition to the stress–strain curves, we have also plotted the linear elastic tangent stiffness curves from immediately before the instability occurs. Fig. 7 reveals that there is a slight influence of nonlinear contributions for all nanowires and these influences appear to be greatest for nanowires with an aspect ratio of 20, despite the compressive buckling strains being less than 1%. Furthermore, it can be seen that the tangent stiffness increases with increasing amounts of compressive strain for the ⟨110⟩/{110}{100} systems, while it decreases for the ⟨100⟩/{100} and ⟨100⟩/{110} systems. This is exactly what happens in Figs. 5 and 6 as the aspect ratio decreases. Moreover, the magnitude of the differences between the tangent modulus before buckling and the Young's modulus is greatest for the ⟨110⟩/{110}{100} system, which is also in accordance with the observations from Fig. 6c. For the ⟨110⟩/{110}{100} system, the tangent modulus immediately before buckling was found to be roughly 13% higher than the Young's modulus for the nanowire with an aspect ratio of 20, which means that the normalized critical force for the aspect ratio 20 nanowire should lie somewhere between 0% and 13% higher than for the aspect ratio 50 nanowire. Inspection of Fig. 6c reveals that the normalized critical force value for the aspect ratio 20 nanowire falls within that range. For the ⟨100⟩/{100} and ⟨100⟩/{110} systems we find that the tangent moduli immediately before buckling were 8% and 6% smaller than the Young's modulus, respectively. Thus, we expect that the maximum deviations in Figs. 6a and b are less than 8% and 6% lower than the asymptotic value, respectively, which also can be confirmed by inspection.

This nonlinear influence also explains why the normalized critical force for a specific cross-sectional size and crystallographic orientation approaches an asymptotic limit value as the aspect ratio increases. This is because the critical strain decreases with increasing aspect ratio and nanowires with large aspect ratios are therefore not influenced by nonlinear elastic properties to the extent that nanowires with small aspect ratios are. Clearly, there is a strong correlation between the deviations from perfectly horizontal behavior in Fig. 6 and the nonlinear elastic behavior in Fig. 7. Hence, it appears to be very likely that the variations in Figs. 5 and 6 for the critical buckling force for a given cross-sectional size are due to a nonlinear elastic contribution to the stiffness. Thus, even though we will not address it here, it is likely that this aspect ratio dependence of the critical force can be systematically modeled by an elastic continuum model.

4.1.3. Wang and Feng buckling model

In addition to comparisons with classical beam theory, we have also compared our results with the buckling model

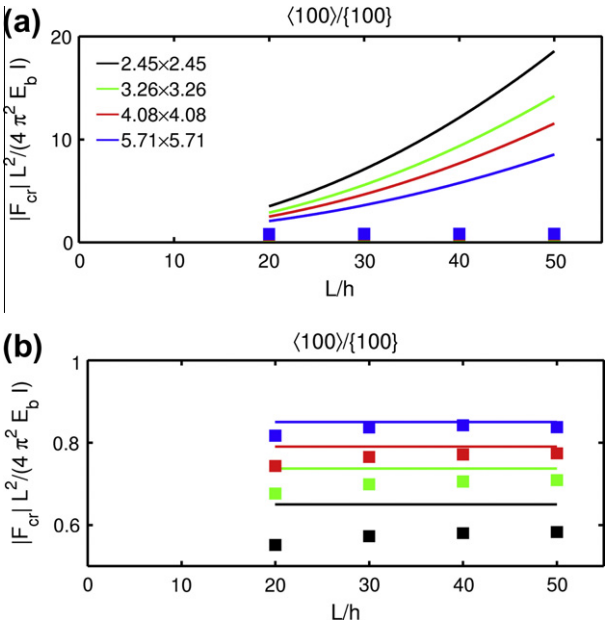

Fig. 8. Comparison of the normalized critical buckling forces from MS simulations and the Wang and Feng model for ⟨100⟩/{100} nanowires with (a) $\tau_0 = 1.33$ J/m^2 and (b) $\tau_0 = 0$. The solid lines correspond to results from the Wang and Feng model and the markers correspond to MS results. (For interpretation to colours in this figure, the reader is referred to the web version of this paper.)

recently proposed by Wang and Feng (WF) [55]. This comparison is of interest because the WF model is based upon the linear surface elasticity theory first proposed by Gurtin and Murdoch [64], in which the surface is assumed be rigidly attached to the bulk, and have its own elastic properties through the following relationship:

$$\tau = \tau_0 + E_s\epsilon, \tag{6}$$

where τ is the surface stress, τ_0 is the residual (strain-independent) surface stress, E_s is the surface stiffness and $E_s\epsilon$ is the strain-dependent surface stress. The various material constants for ⟨100⟩/{100} systems were obtained from our atomistic model, and were found to be $\tau_0 = 1.33$ J/m^2 and $E_s = -4.93$ J/m^2 and Young's modulus for the bulk $E_b = 46.1$ GPa.

Using the WF model for the ⟨100⟩/{100} systems considered here, with square cross-sections and biclamped boundary conditions, the normalized critical force becomes:

$$\frac{|F_{cr}|L^2}{4\pi^2 E_b I} = 1 + \frac{8E_s}{E_b h} + \frac{6}{\pi^2}\left(\frac{\tau_0}{E_b h}\right)\left(\frac{L}{h}\right)^2. \tag{7}$$

In Fig. 8a we have plotted the normalized critical forces from MS simulations and those predicted by the WF model as a function of the aspect ratio. The WF model predicts significant increases in the critical force due to surface effects, up to about 20 times the critical force predicted by the bulk, whereas the MS simulations predict that the critical forces are smaller than those predicted by the bulk. The decrease in normalized critical forces is found to be less than 50% for the MS simulations, significantly different from the increase of the order of 200–2000% predicted by the WF model. For example, for the 2.45 × 2.45 nm^2 nanowires, the WF model predicts that critical forces are 3.5 and 19 times larger than the corresponding bulk values when the aspect ratios are 20 and 50, respectively. This can be compared with the MS results that lie between 50% and 60% of the corresponding bulk value. This suggests that the WF model does not accurately capture the critical buckling forces of nanowires due to surface effects. In particular, from Fig. 8a it can be seen that the discrepancies between the WF model and the MS results increase in a parabolic manner as the aspect ratio increases. This implies that the last term on the right-hand side of Eq. (7), which is the only term that varies with the aspect ratio, accounts for most of the diverging discrepancies between MS results and WF calculations.

To investigate this in more detail we assume that the last term on the right-hand side of Eq. (7) is zero, i.e. $\tau_0 = 0$, to see how well the MS results and the WF calculations agree in such circumstances. In Fig. 8b it can be seen that the agreement between MS results and the WF model is significantly improved when $\tau_0 = 0$. This is in line with observations from other researchers where the eigenfrequency spectrum of silicon nitride cantilevers has been found to be in good agreement with experimental results if $\tau_0 = 0$ [65]. The remaining terms of the right-hand side of Eq. (7) merely constitute the ratio between the size-dependent flexural rigidity and that of the bulk, which implies that the critical force can be modeled through a surface elastic model. It should, however, be noted that a linear elastic uniaxial model in general may be too simple to capture accurately the critical properties. Clearly, it does not capture the nonlinear behavior in Figs. 6 and 7 or any nonlinear relaxation effects, hence it may be necessary to consider this problem with a more general three-dimensional nonlinear elastic surface model.

4.2. Critical buckling strains

In addition to the normalized critical force, we have also studied the equivalent normalized strain, $|\epsilon_{cr}|AL^2/(4\pi^2 I)$, where $|\epsilon_{cr}|$ is the magnitude of the critical strain. Ideally these curves should be horizontal; they should also overlap as the Young's modulus has been eliminated from the equation, and thus all these ratios should be unity. In the same manner as for the critical forces, we also find some variations among the normalized strains (cf. Fig. 9). Some of these variations can be attributed to the perturbation load as it may influence the critical strains somewhat as discussed in Section 3.3. The normalized critical strains are also much more sensitive to variations as they are very small, even for the bulk. Nevertheless, one can distinguish some clear trends. As for the normalized critical forces, it can be seen that the normalized strain curves do not overlap. It is observed that the normalized critical strain decreases with decreasing cross-sectional dimensions. The

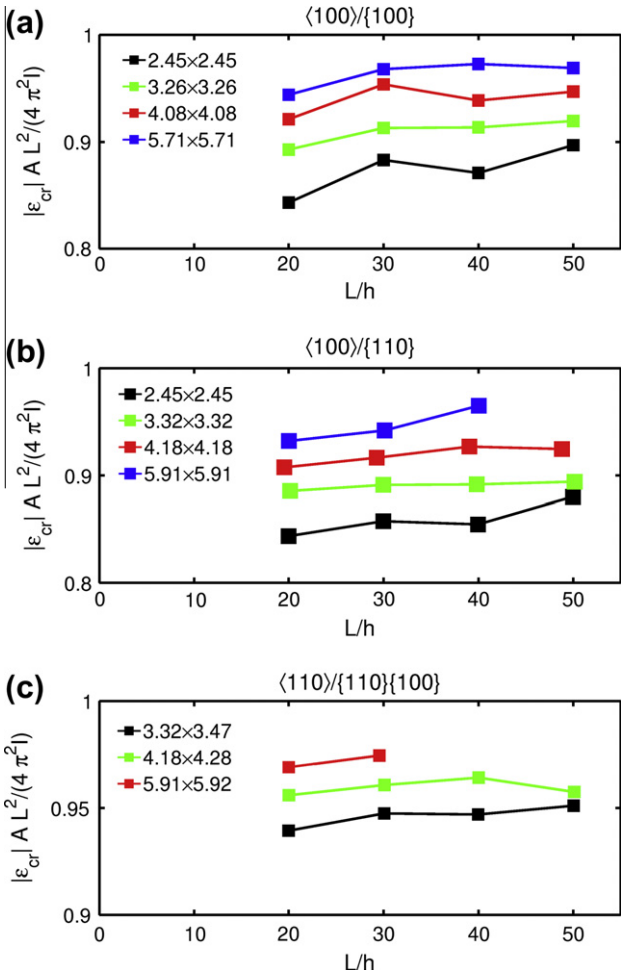

Fig. 9. Normalized critical buckling strain as functions of the aspect ratio for (a) [100]/{100}, (b) [100]/{110} and (c) [110]/{110}{100} systems. (For interpretation to colours in this figure, the reader is referred to the web version of this paper.)

normalized critical strains are closer to unity than the normalized critical forces and the deviations from unity are up to 20%, whereas for the normalized critical forces they are up to 50%.

In Figs. 9a and b we have plotted the normalized critical strains for the ⟨100⟩/{100} and ⟨100⟩/{110} systems, respectively. The magnitudes of the normalized critical strains for the ⟨100⟩/{100} and ⟨100⟩/{110} systems are roughly the same, despite the differences observed for the normalized critical force. Comparing the magnitudes of the normalized critical strains for the ⟨100⟩/{100} and ⟨100⟩/{110} systems with those of the ⟨110⟩/{110}{100} system in Fig. 9c, it can be seen that the strains for the ⟨110⟩/{110}{100} system are much closer to unity.

One possible explanation as to why the different curves do not overlap and why they differ from unity is the simplification of the flexural rigidity. Reducing Eq. (1) to Eq. (3) requires that the flexural rigidity in Eq. (1) can be written as EI, where E and I denote the Young's modulus and moment of inertia, respectively. However, this is not necessarily accurate because the actual definition of the flexural rigidity is given by Eq. (2), which means that in order for $(EI)^* = EI$ to be valid, the Young's modulus must be constant, or homogeneous, over the entire cross-section. However, it has been demonstrated that surfaces have elastic properties that are different to those of the underlying bulk [45,61], which leads to a nanowire cross-section with varying elastic properties. This means that the surfaces that undergo the greatest amounts of strain during bending and have the greatest lever arm from the neutral axis have different elastic properties than the bulk.

It can also be seen that all the critical buckling strains are smaller than their bulk counterparts, which indicates that the surfaces are more compliant than the bulk, which is in agreement with results from previous researchers [45]. Thus it can be expected that the bending moment is overestimated and not accurately described this way, which would explain why the curves in Fig. 9 are not overlapping. The critical strains do nevertheless converge towards those predicted for the bulk when the cross-sectional dimensions increase. The fact that all the obtained strains are smaller than what is predicted by bulk calculations implies that the validity of using Eq. (1) to extract the Young's modulus may not in practice be accurate. Clearly, if the strains are not accurately predicted by Eq. (3), this is a clear indication that $(EI)^* \neq EI$ and that complicates the extraction of the Young's modulus as it cannot be considered a uniform, homogeneous and constant quantity.

We also note that in previous publications we were able to describe the eigenfrequency spectrum of [100]/{100} gold nanowires very accurately without the use of any explicit surface elastic models, which is in contrast to the findings in this paper [35,36]. There are, however, two possible explanations that can shed light on these inconsistencies. First, the considered nanowire sizes in Refs. [35,36] are 4.08×4.08 nm^2 and larger, and the variations in mechanical properties increases quite nonlinearly for smaller nanowires. Thus, we expect larger variations for smaller nanowires. Second, when plane transverse eigenfrequencies of unstressed beams are calculated, these are found to be proportional the square root of the flexural rigidity, i.e. $f_i = k_i\sqrt{(EI)^*}$ [66]. This means that any minor variations in buckling properties due to variations in flexural rigidity will result in even smaller variations when the eigenfrequency spectrum is considered.

4.3. Coupling between normalized critical forces and strains

The observation that the normalized critical strains are smaller than unity may be the explanation for the finding in Section 4.1.1, where it was found that the normalized critical forces were lower than the ratio between the finite-sized Young's modulus and the Young's modulus of the bulk in the limit of large aspect ratios. In fact, there appears to be a correlation between the normalized critical strains, the discrepancies between the ratio of Young's modulus of nanowires and the bulk and the normalized critical forces in the limit of large aspect ratios.

To illustrate this we take the $4.08 \times 4.08\ \mathrm{nm}^2$ nanowire of the $\langle 100\rangle/\{100\}$ system with an aspect ratio of 50. Close inspections of Figs. 6 and 9 reveal that the normalized critical force and strain are 0.77 and 0.95, respectively, and the ratio between the finite-sized Young's modulus and that of the bulk is 0.83. Thus we obtain: $0.83 \cdot 0.95 = 0.79 \approx 0.77$. We performed this type of analysis for nanowires with an aspect ratio of 50 for all the systems and cross-sectional sizes and found that the deviations were in general less than 3%. To describe this in words: (i) we obtain a deviation in the critical strains which we believe is due to the compliant surfaces; and (ii) we have a size-dependent Young's modulus. Together these two discrepancies quite accurately account for the deviations between the normalized critical forces and the ratio between finite-sized and bulk Young's modulus in the limit of large aspect ratios. This is due to the fact that the buckling strains are small for nanowires with large aspect ratios and the influence of nonlinear elastic properties are therefore small. This can be confirmed by inspection of Fig. 7, and shows that the relation between the critical strain and the critical force is close to linear elastic for nanowires with high aspect ratios, where the coefficient of proportion is the size-dependent Young's modulus.

5. Summary and conclusions

In this paper we have studied surface and axial orientation effects on the buckling properties of gold nanowires through MS simulations. As a part of the work we have developed a simple numerical scheme which utilizes small perturbations of the potential energy gradients. This scheme overcomes previously observed numerical complications such as discontinuous stress–strain and energy–strain curves and strain increment size dependencies. It accurately describes the critical forces and strains, and produces an accurate energy transition curve between the initial state and the buckled state. The key findings of this work are:

1. The normalized critical buckling forces are dependent on the axial orientation of the nanowires, where the normalized buckling forces decrease for both the $\langle 100\rangle/\{100\}$ and $\langle 100\rangle/\{110\}$ systems, whereas they increase with decreasing cross-sectional size for the $\langle 110\rangle/\{110\}\{100\}$ system. The critical buckling forces are also dependent on the surface orientation where the $\langle 100\rangle$ wires with $\{100\}$ surfaces had around 8-20% lower critical buckling forces than the $\langle 100\rangle$ wires with $\{110\}$ surfaces depending on the cross-sectional size.
2. The normalized critical buckling forces were found to show deviations from the expected inverse square length dependence for smaller aspect ratio nanowires. This is due to the fact that smaller aspect ratio nanowires require larger strains to induce buckling, which makes the influence of nonlinear elastic properties more important and results in increased and reduced stiffness for $\langle 110\rangle$ and $\langle 100\rangle$ wires, respectively. Overall, this nonlinear elastic influence in stiffness is not as important as the cross-sectional size-dependent Young's modulus in causing deviations of the critical buckling force from the expected bulk value.
3. For the $\langle 100\rangle/\{100\}$ system, we compared our MS results for the critical buckling load with a continuum surface elasticity model recently proposed by Wang and Feng [55]. In contrast to the MS results, the WF model predicted that the critical forces, including nanoscale surface effects, should increase significantly as compared to the critical bulk buckling force, which is in contrast to the MS results which showed that the critical forces decreased compared to the corresponding critical forces of the bulk material.
4. It was found that all the critical buckling strains are lower than their bulk counterparts and that the magnitudes of the critical strains decrease with decreasing cross-sectional dimensions for all surface and axial orientations that were considered. The smaller critical buckling strains are most likely due to the heterogeneous character of the cross-section due to the fact that the surfaces are more compliant than the bulk, which means that these variations must be taken into account when calculating the flexural rigidity. This suggests that the accuracy of Eq. (3) may serve as an indicator as to the validity of using continuum mechanics relationships to extract the Young's modulus from buckling experiments or simulations.
5. Finally, we found a linear elastic correlation between the normalized critical strains and forces for nanowires with high aspect ratios. This suggests that the critical force is close to linearly proportional to the critical strain, and that the constant of proportion is the size-dependent Young's modulus.

Acknowledgments

P.A.T.O. gratefully acknowledges the funding provided by the Swedish research council. H.S.P. gratefully acknowledges the support of NSF Grant 0750395. The simulations were performed using the computational resources at LUNARC, Center for Scientific and Technical Computing, Lund University.

References

[1] Lieber CM, Wang ZL. MRS Bull 2007;32:99.
[2] Park HS, Cai W, Espinosa HD, Huang H. MRS Bull 2009;34:178.
[3] Craighead HG. Science 2000;290:1532.
[4] Wu B, Heidelberg A, Boland JJ. Nat Mater 2005;4:525.
[5] Heidelberg A, Ngo LT, Wu B, Phillips MA, Sharma S, Kamins TI, et al. Nano Lett 2006;6:1101.
[6] Cuenot S, Frétigny C, Demoustier-Champagne S, Nysten B. Phys Rev B 2004;69:165410.

[7] Jing GY, Duan HL, Sun XM, Zhang ZS, Xu J, Li YD, et al. Phys Rev B 2006;73:235409.
[8] Nilsson SG, Sarwe EL, Montelius L. Appl Phys Lett 2003;83:990.
[9] Nilsson SG, Borrisé X, Montelius L. Appl Phys Lett 2004;85:3555.
[10] Lavrik NV, Sepaniak MJ, Datskos PG. Rev Sci Instrum 2004;75:2229.
[11] Zhu Y, Xu F, Qin Q, Fung WY, Lu W. Nano Lett 2009;9:3934.
[12] Han X, Zheng K, Zhang Y, Zhang X, Zhang Z, Wang ZL. Adv Mater 2007;19:2112.
[13] Ekinci KL, Roukes ML. Rev Sci Instrum 2005;76:061101.
[14] Ekinci KL, Huang XMH, Roukes ML. Appl Phys Lett 2004;84:4469.
[15] Yang YT, Callegari C, Feng XL, Ekinci KL, Roukes ML. Nano Lett 2006;6:583.
[16] Gupta A, Akin D, Bashir R. Appl Phys Lett 2004;84:1976.
[17] Viani MB, Schäffer TE, Chand A, Reif M, Gaub HE, Hansma PK. J Appl Phys 1999;86:2258.
[18] Ilic B, Czaplewski D, Craighead HG, Neuzil P, Campagnolo C, Batt C. Appl Phys Lett 2000;77:450.
[19] Stowe TD, Yasumura K, Kenny TW, Botkin D, Wago K, Rugar D. Appl Phys Lett 1997;71:288.
[20] Petrova H, Perez-Juste J, Zhang Z, Zhang J, Kosel T, Hartland GV. J Mater Chem 2006;16:3957.
[21] Lexholm M, Karlsson I, Boxberg F, Hessman D. Appl Phys Lett 2009;95:113103.
[22] Husain A, Hone J, Postma HWCh, Huang XMH, Drake T, Barbic M, et al. Appl Phys Lett 2003;83:1240.
[23] Cimalla V, Foerster Ch, Will F, Tonisch K, Brueckner K, Stephan R, et al. Appl Phys Lett 2006;88:253501.
[24] Verbridge SS, Parpia JM, Reichenbach RB, Bellan LM, Craighead HG. J Appl Phys 2006;99:124304.
[25] Verbridge SS, Finkelstein Shapiro D, Craighead HG, Parpia JM. Nano Lett 2007;7:1728.
[26] Riaz M, Nur O, Willander M, Klason P. Appl Phys Lett 2008;92:103118.
[27] Ji LW, Young SJ, Fang TH, Liu CH. Appl Phys Lett 2007;90:033109.
[28] Young SJ, Ji LW, Chang SJ, Fang TH, Hsueh TJ, Meen TH, et al. Nanotechnology 2007;18:225603.
[29] Lin CH, Ni H, Wang X, Chang M, Chao YJ, Deka JR, et al. Small 2010;6:927.
[30] Lu Y, Huang JY, Wang C, Sun S, Lou J. Nat Nanotechnol 2010;5:218.
[31] Kim SY, Park HS. Appl Phys Lett 2009;94:101918.
[32] Kim SY, Park HS. Phys Rev Lett 2008;101:215502.
[33] Rogers JA, Someya T, Huang Y. Science 2010;327:1603.
[34] Baca AJ, Ahn JH, Sun Y, Meitl MA, Menard E, Kim HS, et al. Angew Chem Int Ed 2008;47:5524.
[35] Olsson PAT. J Appl Phys 2010;108:034318.
[36] Olsson PAT, Park HS, Lidström PC. J Appl Phys 2010;108:104312.
[37] Olsson PAT, Melin S, Persson C. Phys Rev B 2007;76:224112.
[38] Park HS, Zimmerman JA. Phys Rev B 2005;72:054106.
[39] Park HS, Gall K, Zimmerman JA. Phys Rev Lett 2005;95:255504.
[40] Park HS, Gall K, Zimmerman JA. J Mech Phys Solids 2006;54:1862.
[41] Diao J, Gall K, Dunn ML. Nat Mater 2003;2:656.
[42] Diao J, Gall K, Dunn ML. Nano Lett 2004;4:1863.
[43] Diao J, Gall K, Dunn ML. Phys Rev B 2004;70:75413.
[44] Zhou LG, Huang H. Appl Phys Lett 2004;84:1940.
[45] Liang H, Upmanyu M, Huang H. Phys Rev B 2005;71:241403(R).
[46] McDowell MT, Leach AM, Gall K. Modell Simul Mater Sci Eng 2008;16:045003.
[47] Wang ZG, Li JB, Gao F, Weber WJ. Acta Mater 2010;58:1963.
[48] Wang ZG, Zu X, Yang L, Gao F, Weber WJ. Physica E 2008;40:561.
[49] Wen YH, Wang Q, Liew KM, Zhu ZZ. Phys Lett A 2010;374:2949.
[50] Wen YH, Zhang Y, Wang Q, Zheng JC, Zhu ZZ. Comput Mater Sci 2010;48:513.
[51] Jiang W, Batra RC. Acta Mater 2009;57:4921.
[52] Makeev MA, Srivastava D, Menon M. Phys Rev B 2006;74:165303.
[53] Cao G, Chen X. Nanotechnology 2006;17:3844.
[54] Wang Z, Zu X, Gao F, Weber WJ. Phys Rev B 2008;77:224113.
[55] Wang GF, Feng XQ. Appl Phys Lett 2009;94:141913.
[56] Timoshenko SP, Gere JM. Theory of elastic stability. 2nd ed. New York: McGraw-Hill; 1961.
[57] Bitzek E, Koskinen P, Gähler F, Moseler M, Gumbsch P. Phys Rev Lett 2006;97:170201.
[58] See supplementary material to Ref. [35] at <http://www.dx.doi.org/10.1063/1.3460127> for the parametrization of the EAM potential.
[59] Ackland GJ, Jones AP. Phys Rev B 2006;73:054104.
[60] Li J. Modell Simul Mater Sci Eng 2003;11:173.
[61] Dingreville R, Qu J, Cherkaoui M. J Mech Phys Solids 2005;53:1827.
[62] Dingreville R, Kulkarni AJ, Zhou M, Qu J. Modell Simul Mater Sci Eng 2008;16:025002.
[63] Wang CM, Wang CY, Reddy JN. Exact solutions for buckling of structural members. Boca Raton (FL): CRC Press; 2005.
[64] Gurtin ME, Murdoch AI. Arch Ration Mech Anal 1975;57:291.
[65] Gavan KB, Westra HJR, van der Drift EWJM, Venstra WJ, van der Zant HSJ. Appl Phys Lett 2009;94:233108.
[66] Géradin M, Rixen D. Mechanical vibrations. 2nd ed. New York: Wiley; 1997.